

# A Novel UWB-based Multilateration Technique for Indoor Localisation

Oladimeji Onalaja, *Student Member, IEEE*, Mounir Adjrad, *Member, IEEE* and Mohammad Ghavami, *Senior Member, IEEE*

**Abstract**—In this paper, we present a novel geometrically driven multilateration technique that is based on Ultra-Wideband (UWB) technology. We refer to our proposed solution as Time Reflection of Arrival (TROA). We demonstrate in this paper that the position estimation error is improved upon by carefully considering the inherent properties of the UWB technology and the reflection properties of transmitted UWB signals. By a direct comparison between TROA and two widely used multilateration techniques, we show that indoor position estimation can be done much more effectively using our proposed solution. We also derive a new Cramér-Rao lower bound (CRLB) for TROA multilateration and use it to show its level of efficiency.

**Index Terms**—UWB, Indoor Position Estimation, TROA, Multipath propagation, Geometric Multilateration

## I. INTRODUCTION

POSITION estimation problems have seen an exponentially increased interest in recent years [1-7]. Position estimation techniques are generally based on two underlying principles namely: ‘Geometric Multilateration’ and ‘Statistical Multilateration’ [8-9]. Geometric multilateration techniques estimate position by using the geometrical link resulting of signal propagation between a node of interest (NOI), neighbouring reference nodes and base stations. Its variants include time of arrival (TOA), time difference of arrival (TDOA), time sum of arrival (TSOA), the received signal strength (RSS) and the angle of arrival (AOA) [1-4;8-9]. Statistical multilateration techniques such as [5-7], estimate position by means of statistical modelling of error bounds and other stochastic models. TSOA based multilateration techniques have seemingly not made the cut with regards to potential accuracy enablers. As [8-9] and [11] explain, the general consensus seems to be that they do not provide any additional performance advantage(s) over other widely used hyperbolic based multilateration techniques. In this work, we prove this theory to be right by means of a direct comparison with the TOA multilateration technique as well as our proposed technique. However; and much more significantly, in this work, we build-up on the fundamental working principles of the TSOA based multilateration technique; and use it to derive a novel technique which we coin as time reflection of arrival (TROA). We derive a theoretical lower bound on the covariance of the TROA estimator based on the Cramér-Rao

lower bound (CRLB); and show that our proposed approach achieves relatively good operational performances when the Mean Squared Error (MSE) implications are considered. The rest of this paper is organised as follows: Section II details an introduction into the concept of TSOA multilateration; Section III illustrates our proposed system’s basic functionality right from its initial conception; and also bridges any inadvertent knowledge gap between its conceptualisation, practical ramifications and theoretical accuracy. Section IV discusses the UWB channel modelled for the proposed TROA multilateration scheme; Section V validates our system by means of simulation results and CRLB analysis; and Section VI summarises and concludes this work.

## II. BACKGROUND

TSOA multilateration involves the propagation of signals from a NOI to known and fixed reference nodes ( $RN_{i=1,2,3,\dots,\infty}$ ) or anchors [8]. The reference nodes are typically receivers; and conventionally, the NOI is required to be either active (i.e. a mobile station) or semi-passive (i.e. a semi-passive radio frequency identification (RFID) tag); or alternatively have an inherently active or semi-passive component that facilitates its signal propagation to the various reference nodes required for multilateration [8-9]. As depicted in Fig. 1, following the signal propagation from the NOI, two reference nodes are usually paired together to generate a range sum estimate. This range sum estimate is then used to define a conic section whose semi-major axis is always greater than its semi-minor axis (i.e. an ellipse) [10]. With reference to Fig. 1; and considering the pairing between  $RN_1$  and  $RN_2$ , the range sum is defined as the algebraic sum of  $D_{NOI-RN_1}$  (distance between NOI and  $RN_1$ ) and  $D_{NOI-RN_2}$  (distance between NOI and  $RN_2$ ). Assuming a line-of-sight (LOS) separation between the NOI and both reference nodes,  $D_{NOI-RN_1}$  and  $D_{NOI-RN_2}$  are determined by multiplying the arrival time of the propagated signal at the respective nodes by  $c$  (speed of light). The general equation for the defined ellipse ( $E_i$ ) based on the range sum is given by (1) where  $(h_1, k_1)$  is its center coordinate,  $a_1$  is its semi-major axis; and  $b_1$  is its semi-minor axis [10].

$$\frac{(x_i - h_i)^2}{a_i^2} + \frac{(y_i - k_i)^2}{b_i^2} = 1 \quad (1)$$

Denoting  $E_1$  of center coordinate  $(h_1, k_1)$ , semi-major axis  $a_1$ ; and semi-minor axis  $b_1$  as the ellipse defined by the pairing between  $RN_1$  and  $RN_2$ , when a third reference node ( $RN_3$ ) is introduced and paired with  $RN_2$  just as Fig 2. depicts, another

Manuscript received September 11, 2013.

The authors are with the Biomedical Engineering and Communications (BiMEC) Research Group, Department of Engineering and Design, Faculty of Engineering, Science and the Built Environment at London South Bank University, London, SE1 0AA, United Kingdom (email: {onalajao, ghavami, adjradm}@lsbu.ac.uk)

ellipse ( $E_2$ ) with center coordinate  $(h_2, k_2)$ , semi-major axis  $a_2$ ; and semi-minor axis  $b_2$  is defined. Based on the fact that the definition of both  $E_1$  and  $E_2$  are dependent on the common NOI, their intersection will *always* result in a set of intersection points ( $I_p$ ) of which one set inadvertently identifies the position of the NOI. However and with reference to Fig. 2, identifying the intersection point that denotes the exact position of the NOI tends to become a cumbersome task when the intersection between  $E_1$  and  $E_2$  results in more than two (2)  $I_p$ . Ultimately, the need for a practical way to differentiate intersection coordinates between  $E_1$  and  $E_2$  that defines the position of the NOI from those that come about as a direct consequence of the general geometry arises. To this effect, the classical trilateration process which is a feature of most hyperbolic driven positioning techniques is usually invoked [8]. In general, trilateration is a multilateration process that locates a NOI using exactly three vantage points ( $VP_{i=1,2,3}$ ).

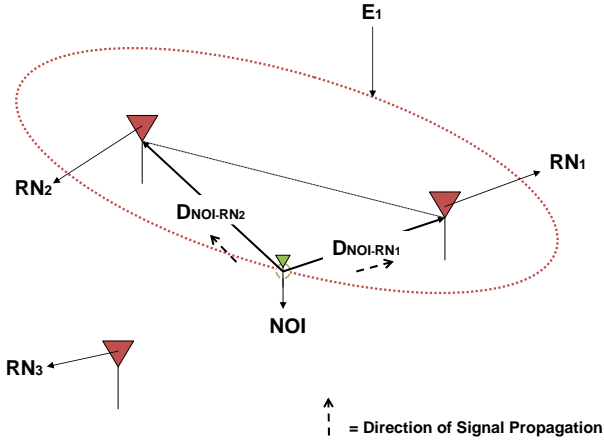


Fig. 1: Generation of a single ellipse using two RN's

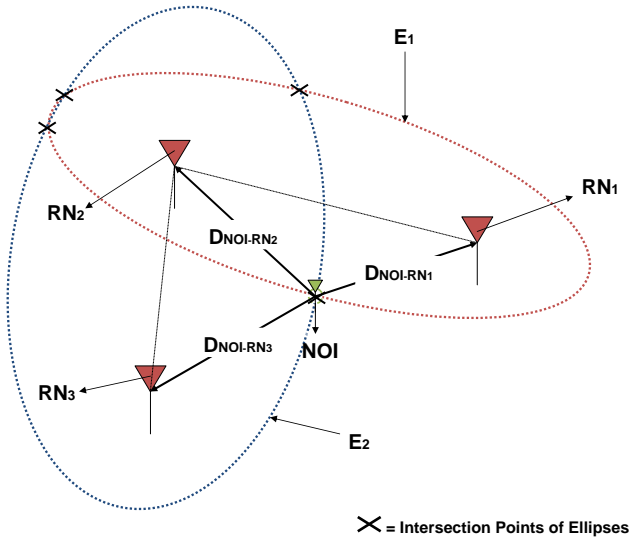


Fig. 2: Generation of two ellipses using three RN's

In the scenario depicted by both Figs. 1 and 2,  $VP_1$  would be the reference node pairing between  $RN_1$  and  $RN_2$  that defines  $E_1$ ; and  $VP_2$  would be the reference node pairing between

$RN_2$  and  $RN_3$  that defines  $E_2$ . Introducing a third vantage point just as the trilateration process postulates introduces a third ellipse which brings us a step closer to resolving the 'coordinate of the NOI' ambiguity problem. By introducing another reference node  $RN_4$ , and considering the vantage point that would bring about the pairing between itself and any of the previously defined three reference nodes, a third ellipse  $E_3$  with center coordinate  $(h_3, k_3)$ , semi-major axis  $a_3$ ; and semi-minor axis  $b_3$  is defined. As before, by virtue of all three ellipses definition dependence on the NOI, there will be one common coordinate between all three ellipses when they intersect. However, when they do intersect, there will be quite a number of intersection coordinates between the vantage point pairings but there will only be one unique intersection coordinate for the intersection of all three conic sections. That unique coordinate of intersection is  $(x_{noi}, y_{noi})$  and as a consequence, the location of the NOI. At this junction, it is noteworthy to mention that the success of the described trilateration process is partially dependent on the proper placement of the reference nodes in a defined indoor environment prior to its execution [9]. Having mentioned that, a clear guide to the proper placement of reference nodes in a defined environment; as well as the inadvertent limitations that comes with it, is yet to be proposed in any literature.

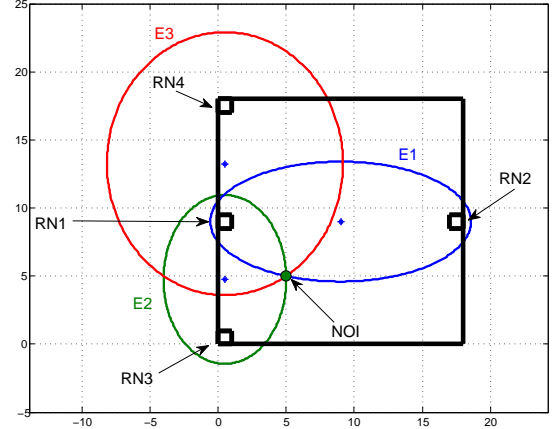


Fig. 3: Generation of two ellipses using three RN's

Fig. 3 depicts the aerial view of a typically effective placement configuration of all four reference nodes required for the trilateration process. The reference node pairings  $RN_1 - RN_2$ ,  $RN_1 - RN_3$  and  $RN_1 - RN_4$  assume the form of  $VP_1$  ( $E_1$ ),  $VP_2$  ( $E_2$ ) and  $VP_3$  ( $E_3$ ) respectively; and the TSOA trilateration process is completed accordingly to determine the coordinates of the NOI [8].

### III. PROPOSED TIME REFLECTION OF ARRIVAL (TROA) TECHNIQUE

#### A. The Optimum 2D Solution Space

The 2D solution space of our proposed system is optimised for position estimation in both a square and rectangular shaped indoor environment; and its setup in both quadrilaterals are depicted in Fig. 4. Prior to its setup in the environment, the value of 'A' which would intuitively always be the largest distance

in both quadrilaterals, is determined ( $A = \sqrt{2L^2}$  for the square and  $A = \sqrt{L^2 + B^2}$  for the rectangle where  $L$  and  $B$  are the respective Lengths and Breadths of the quadrilaterals). This is done to ensure that all signal propagation in both cases is within the indoor UWB transmission range ( $R_{UWB}$ ) which is typically less than or equal to 30m [12]. To this effect, we define any squared or rectangular shaped indoor environment that satisfies the condition of  $A \leq R_{UWB}$  as our ‘Optimum 2D Solution Space (O2SS)’. In an event of the TROA system being setup outside the O2SS, there will be regions with no signal propagation; and this would lead to a high reduction in the performance of the system and ultimately a failure of the localisation task.

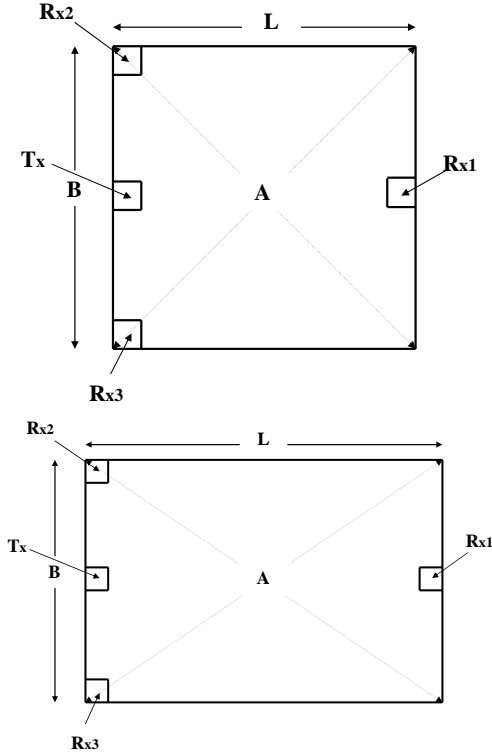


Fig. 4: Aerial View of TROA System setup for a square and rectangular shaped indoor environment

### B. TROA Multilateration

In contrast to both the conventional TOA and TSOA based multilateration techniques that require either an active or a semi-passive NOI to enable signal propagation from it (the NOI) to the relevant reference nodes, TROA is conceived to rely wholly on an inherently passive NOI. In most indoor residential applications, the NOI tends to range from secondary targets such as key electrical appliances and other non-electronic devices to much more primary and inherently animate targets such as the human body. For position estimation using our proposed method, the NOI which could either be a primary or secondary target is equipped with a passive lightweight material of known electrical properties (i.e. conductivity, permittivity, loss tangent, dielectric constant). In

[13], we showed that based on the reflection properties of UWB signals as well as having a priori knowledge of the electrical properties of the material that is used to make up an object of interest (lightweight material attached to the NOI in this scenario), it is possible to determine and predict the expected reflected waveform at any UWB receiver (reference node in this scenario) when a UWB signal is incident on the said object of interest. Taking this into consideration, TROA multilateration is initially defined in accordance with that which is depicted in Fig. 5. With reference to Fig. 5, TROA replaces TSOA’s dependence on  $RN_1$  and  $RN_2$  with a UWB transmitter ( $T_x$ ); and a UWB receiver ( $R_x$ ) respectively. When  $T_x$  transmits a UWB signal, a version of it will be received at  $R_x$  by virtue of the LOS provisioning at a distance of  $D_{LOS}$ ; and after a time delay which is brought about by the reflection of the UWB signal off the lightweight material attached to the NOI, a version of the signal is also received at  $R_x$ .

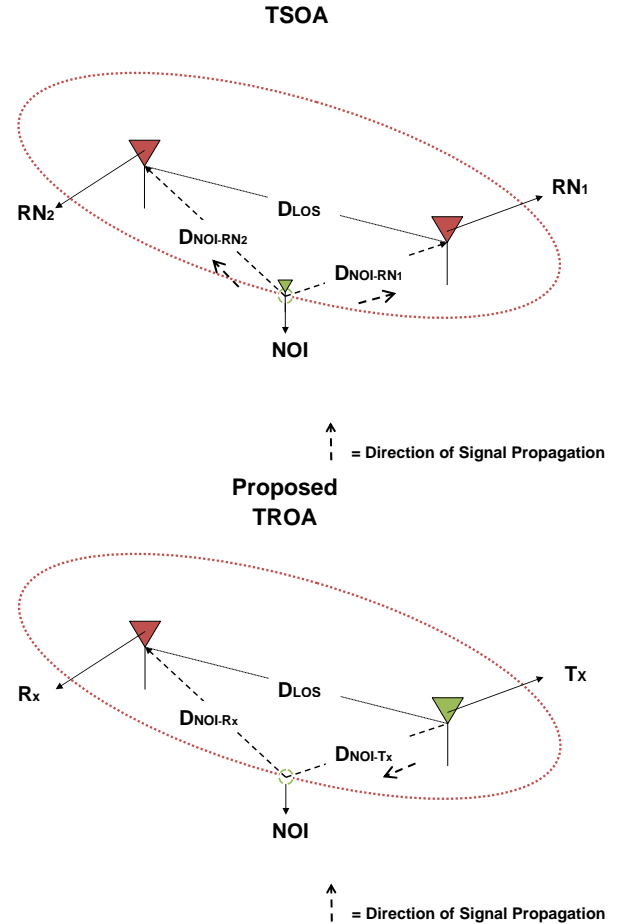


Fig. 5: Generation of ellipses using TSOA and TROA Multilateration approaches

Considering a simplistic albeit realistic two-path propagation model and a square shaped indoor environment, once the environment gets tested for compliance with the O2SS requirement and passes it (i.e.  $A \leq R_{UWB}$ ), a transmitter ( $T_x$ ) and three receivers ( $R_{x1}$ ,  $R_{x2}$  and  $R_{x3}$ ) are deployed in the square as thus. Likening  $L$  and  $B$  which is defined in Fig. 4 to the typical  $x$  and  $y$  axis on a 2D  $x$ - $y$  grid respectively,

$T_x$  is deployed at coordinate  $(0.5p, 0.5L)$ ,  $R_{x1}$  is deployed at coordinate  $(L-0.5p, 0.5L)$ ,  $R_{x2}$  is deployed at coordinate  $(0.5p, L-0.5p)$ ; and  $R_{x3}$  is deployed at coordinate  $(0.5p, 0.5p)$  where  $p$  is strictly an arbitrary positive integer that enforces a displacement of both the transmitter or receiver from the edges of the O2SS.

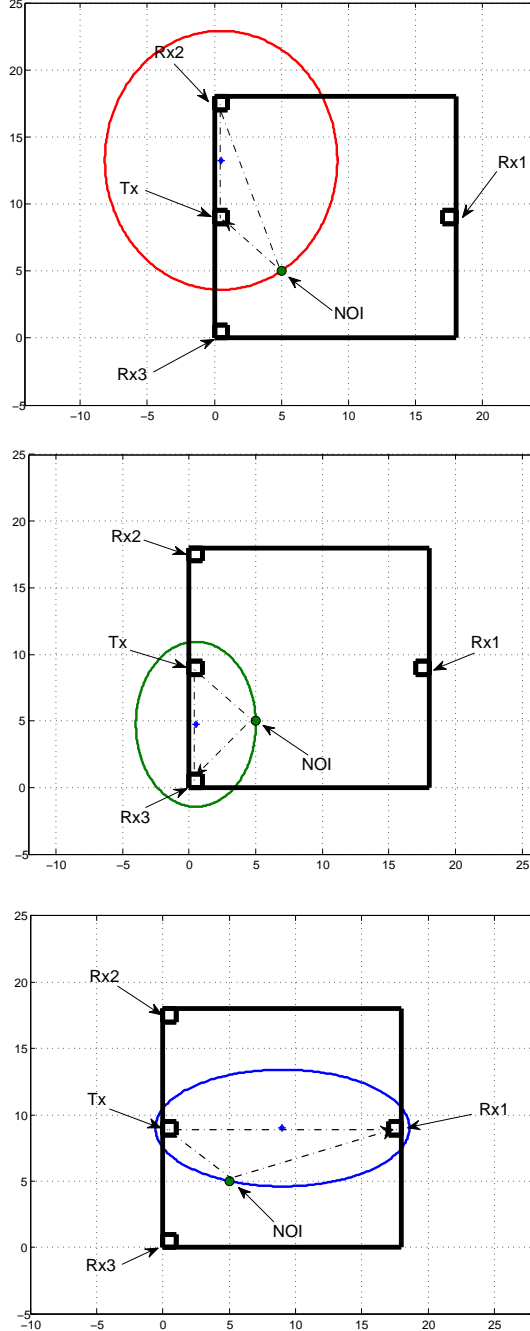


Fig. 6: Generation of ellipses using proposed TROA approach

In liaison with Fig. 6,  $VP_1$  becomes the pairing between  $T_x$  and  $R_{x2}$  while  $VP_2$  and  $VP_3$  becomes the pairings between  $T_x$  and  $R_{x3}$ ; and  $T_x$  and  $R_{x1}$  respectively.  $D_{LOS1}$ ,  $D_{LOS2}$  and  $D_{LOS3}$  are the respective LOS separation distances between the  $VP_1$ ,  $VP_2$  and  $VP_3$  pairings. Considering  $VP_1$ , when an UWB signal

$x(t)$  is transmitted by  $T_x$ ,  $x'(t)$  is received by  $R_{x2}$  at time  $t_1$  by virtue of the LOS provisioning. At time  $t_2$ ,  $s(t)$  is also received by  $R_{x2}$  by virtue of  $x(t)$  reflecting off the NOI. Since  $\alpha$  is the time delay between the reception of  $x'(t)$  and  $s(t)$ , considering the ideal nature of the assumed environment,  $\alpha$  is determined signal processing-wise by means of cross correlating  $s(t)$  and  $x(t)$  (i.e.  $R_{sx}(\tau)$ ). A simple plot of  $R_{sx}(\tau)$  will lead a single peak occurring at the point where  $\tau = \alpha$ ; and hence the value of  $\alpha$  can be easily deduced from the plot. However this can only be done by an initial estimation of  $s(t)$  which is achieved by a convolution between  $x(t)$ , the impulse response of the indoor UWB channel  $h(t)$  and the reflection coefficient of the UWB signal  $r(t)$  [12]. A multiplication of  $\alpha$  with  $c$  and then adding it to  $D_{LOS1}$ , generates the ‘range sum’ associated with  $VP_1$ . Repeating the same process for both  $VP_2$  and  $VP_3$  generates the range sum associated with it too.

### C. Conic Section Definition and NOI Identification

With reference to the general equation of an ellipse given by (1); and taking all three vantage points into consideration, ‘ $a_i$ ’ is defined as half the range sum (i.e., range sum/2); and ‘ $b_i$ ’ is defined as  $a_i\sqrt{1-e_i^2}$  where ‘ $e_i$ ’ denotes the eccentricity of the ellipse.  $e_i$  in turn is defined as  $f_i / a_i$  where ‘ $f_i$ ’ is half the distance between the two foci of the ellipse. Consequently, ‘ $f_i$ ’ can be re-defined as half the distance between the LOS separation between  $T_x$  and the corresponding receivers (i.e.  $f_1 = D_{LOS1}/2$  for  $VP_1$ ,  $f_2 = D_{LOS2}/2$  for  $VP_2$  and  $f_3 = D_{LOS3}/2$  for  $VP_3$ ). Just as Fig. 6 depicts it, for all three vantage points, three ellipses  $E_1$ ,  $E_2$  and  $E_3$  which are respectively centered at  $(0.5p, ((L - 0.5) + (L/2))/2)$ ,  $(0.5p, 0.5f_2)$  and  $(0.5f_3, 0.5L)$  are constructed accordingly. Usually, at this stage of the multilateration process, trilateration is invoked to determine the coordinate of the NOI just as we discussed earlier for the TSOA scenario. However, for our proposed TROA, we perform the trilateration process in a non-conventional manner by a series of elliptical grouping and subsequent comparison. Essentially, the coordinate of the NOI’s location is determined by an initial grouping of the defined ellipses; and thereafter a direct comparison of their intersection points for similarities. For a given execution cycle, ellipses  $E_1$  and  $E_2$  are grouped; and their intersection coordinates  $\{(x(1), y(1)) \text{ and } (x(2), y(2))\}$  are determined. In a similar manner, ellipses  $E_1$  and  $E_3$  are also grouped; and their intersection coordinates  $\{(x(3), y(3)) \text{ and } (x(4), y(4))\}$  are also determined. With a combination of four intersection coordinates determined for both groupings, the current execution cycle is concluded by identifying a pair of coordinates in both groups that have similar values. This identified similar values inadvertently denotes the coordinate of the NOI; and ultimately its location in the given indoor environment.

## IV. UWB COMMUNICATION CHANNEL CONSIDERATION

### A. The UWB Transmit Signal

The UWB transmit signal  $x(t)$  depicted in Fig. 7 typically takes the form of the second derivate of the Gaussian impulse function; and (2) gives its mathematical representation [9,14].

$$x(t) = \left(1 - 16\pi \left(\frac{t}{\Delta T}\right)^2\right) e^{-8\pi(t/\Delta T)^2} \quad (2)$$

$\Delta T$  is defined as the nominal time duration of  $x(t)$  and it is usually set to a value of 0.2 ns (nanoseconds) in a bid to adhere to the stringent mask set by the Federal Communications Commission (FCC) for any signal propagation within the unlicensed UWB communications band [9,14]. Essentially, setting  $\Delta T$  to the aforementioned value results in a -3dB bandwidth that spans from 5 GHz to 11.5 GHz which lies well within the allocated communications band (3.1 GHz to 10.6 GHz); and thus making  $x(t)$  a UWB signal [9].

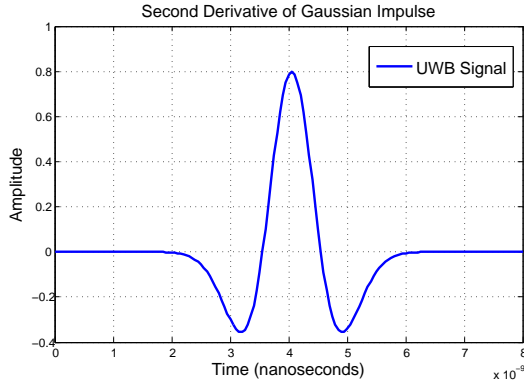


Fig. 7: UWB Signal: Second derivative of Gaussian Impulse

### B. The UWB Channel Model

Generally, there are two approaches taken in the modelling of the UWB communication channel namely the widely known and accepted empirical approach [12,15-16] and the physics-based approach [15-16]. In contrast to the physics-based approach; and due to the inadvertent complexity in modelling pulse distortions, empirical approaches are not readily available in a generalized closed form; and this is where physics-based modelling comes into play [16]. At this junction, it is noteworthy to mention that in physics, signal distortions due to reflections are fundamentally dissimilar to signal distortions due to diffraction [16].

From a multilateration vantage point, the parameter of utmost importance is the first arriving multipath component (MPC) of the originally transmitted UWB signal [8-9]. Nevertheless, the successful detection and subsequent estimation of this MPC at a receiver end is in most cases significantly hindered by the environmentally driven reflections and diffractions. This hindrance brings about a need to model the UWB communication channel in an attempt to cater for the destructive effects (i.e. pulse distortions) reflections and diffractions will have on the transmitted UWB signal. The physics-based approach models the indoor UWB communication channel as a collation of individually localized scattering centre ( $S_{i=1,2,3,\dots,\infty}$ ) models similar to that which Fig. 8 depicts.

For the distortion model depicted in Fig. 8 which typifies the conventional and well studied two-ray indoor communications

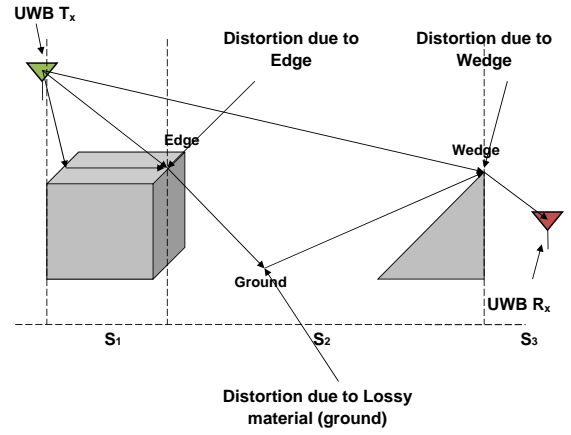


Fig. 8: Physics-based pulse distortion model

model that is used in a lot of UWB applications, there are three scattering centres ( $S_{i=1,2,3}$ ); and each of them characterises the distortion of the UWB signal in its region by means of the impulse response of the UWB signal to the reflection or diffraction brought about by the surrounding inanimate object(s). The characteristic impulse response that corresponds to each of the scattering centres are well documented in [15-16]. Additionally, at any given time, the arrival path of the UWB signal into scattering centre  $S_i$  is governed by the departure trajectory of the signal arriving from the preceding scattering centre (i.e.  $S_{i-1}$ ).

Having said that, for this work we focus wholly on and base the modelling of the UWB communications channel entirely on the physics-based approach that relates to  $S_2$  in Fig. 8 when it is considered as an isolated scattering centre. As shown in Fig. 9, for our channel model, the dependency of the arrival path of the UWB signal on the departure trajectory of the signal from the preceding scattering centre is replaced by a fixed omni-directional UWB transmitter ( $T_x$ ).  $T_x$  and the respective receivers are placed at the corners of the ceiling of a defined O2SS just as Fig. 9 depicts it at specific coordinates which we defined in verbatim in the previous section. With reference to [16] and considering the vantage point that pairs  $T_x$  with  $R_{x1}$  (i.e.  $VP_3$  from the previous section), for non-zero values of the incidence angle  $\psi$  of the transmitted UWB signal  $x(t)$  where  $\epsilon_r$  and  $\sigma$  refer to the relative dielectric constant of the lossy material and its conductivity respectively, the transfer function and its analogous impulse response  $h(\tau)$  associated with  $x(t)$  when it suffers some distortion pulse-wise in a scattering centre similar to  $S_2$  is as a direct consequence of Geometric Optics (GO) Rays (i.e. reflection off the lossy material); and is defined as:

$$h(\tau) = \frac{1}{r_1} \delta(\tau) + \frac{1}{r_2} R_1(\tau) \otimes \delta(\tau - \tau_1) \quad (3)$$

where  $R_1(t) = \pm K\delta(t) + R_{01}(t)$ ,  $R_{01}(t)$  which in turn is defined as the reflection coefficient of the transmitted UWB signal is denoted by:

$$R_{01}(t) = \left(\frac{4k}{1-k^2}\right) \left(\frac{e^{-at}}{t}\right) \sum_{n=1}^{\infty} (-1)^{n+1} n K^n I_n(at),$$



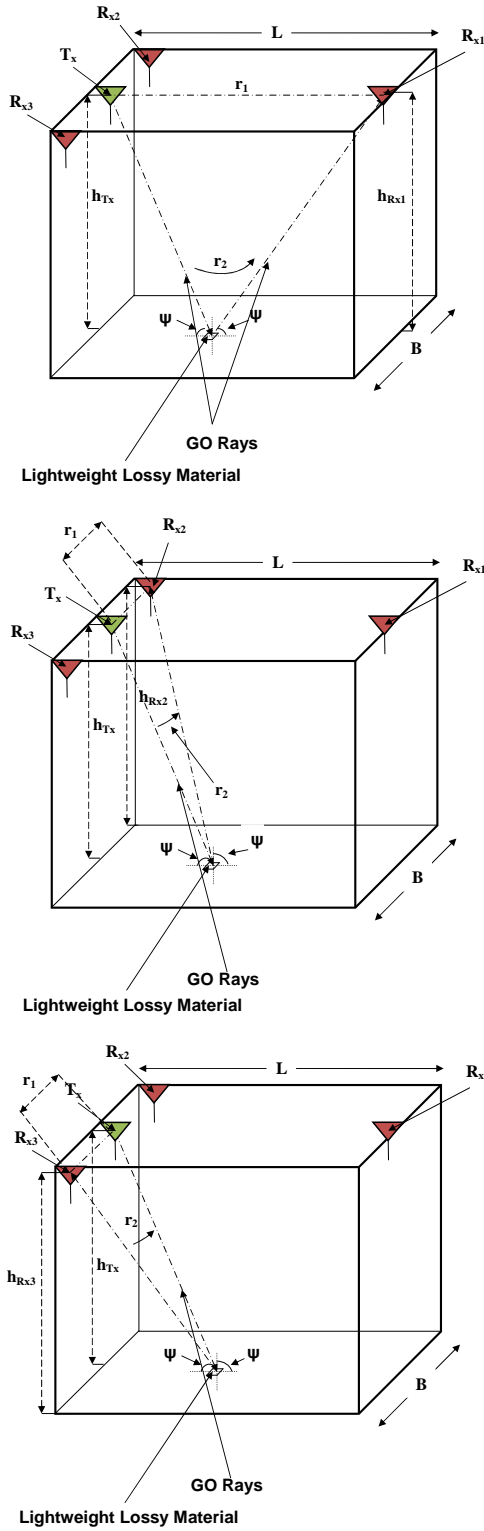


Fig. 9: UWB Channel Model description for proposed TROA

$$\tau_1 = \frac{(r_2 - r_1)}{c}, K = \frac{(1-k)}{(1+k)},$$

$$k = \begin{cases} \sqrt{\epsilon_r - \cos^2 \psi} / (\epsilon_r \sin \psi) & \text{for vertical polarization} \\ \sin \psi / \sqrt{\epsilon_r - \cos^2 \psi} & \text{for horizontal polarization} \end{cases}$$

$$\psi = \arctan \frac{(h_{T_x} + h_{R_x})}{d}, r_1 = \sqrt{(h_{T_x} - h_{R_x})^2 + d^2},$$

$$r_2 = \sqrt{(h_{T_x} + h_{R_x})^2 + d^2}, a = \frac{120\pi\sigma c}{2\epsilon_r}$$

Just as [18-19] have pointed out extensively, based on the fact that  $I_n(at)$  is the modified Bessel function, for values of  $at \leq 1$ ,  $R_{01}(t)$  can be manipulated and finally reduced to:

$$R_{01}(t) \approx K \frac{2k}{1-k^2} e^{-(1+K)at}$$

Without loss of generality, in our indoor environment and with reference to Fig. 9, the values of  $h_{T_x}$ ,  $h_{R_{x1}}$ ,  $h_{R_{x2}}$  and  $h_{R_{x3}}$  are the same; and hence  $\psi$ ,  $r_1$  and  $r_2$  can all be respectively re-defined as:

$$\psi = \arctan \frac{2h}{d}, r_1 = d, r_2 = \sqrt{2h^2 + d^2}$$

where

$$h = h_{T_x} = h_{R_{x1}} = h_{R_{x2}} = h_{R_{x3}}$$

It suffices to say that the impulse response definition for the vantage point that pairs  $T_x$  with  $R_{x1}$  also follows through from the other two vantage points that pairs  $T_x$  with  $R_{x3}$  and  $R_{x2}$  respectively just as Fig. 9 illustrates.

## V. VALIDATION OF TECHNIQUE

### A. TROA vs. TOA vs. TSOA (Effectiveness Test)

Innately, the effectiveness of any geometric multilateration technique relies heavily on the accuracy of the initially obtained TOA measurements. It suffices to hypothesise that a necessary comparison between two or more multilateration techniques in an attempt to determine their order of effectiveness becomes one that has to be driven by an introduced and calculated variation in the TOA measurements. To this effect; and considering LOS propagation conditions, we modelled this TOA measurement variation for all three methods (i.e., TROA, TOA and TSOA) as a normally distributed Gaussian random variable  $N(0, \sigma^2)$ ; and generated 1000 random samples each for a fixed range of standard deviation ( $\sigma$ ) of the TOA measurements. This range of  $\sigma$  was fixed to coincide with a localisation accuracy that spans from 3 cm to 30 cm (i.e., 0.1 ns to 1 ns). We subjected the NOI to a number of fixed coordinates and for demonstration purposes in this paper, we focus on and present the results for three randomly picked coordinates namely (5,5), (9,14) and (12,4).

The initial TOA measurements that result in the determination of all three defined coordinates using TROA, TOA and TSOA are respectively corrupted with the randomly generated Gaussian noise samples over the defined  $\sigma$  range; and the NOI's location is subsequently redetermined. Figs. 10, 11 and 12 show the resultant  $\sigma$  vs. mean squared error (MSE) plots for the specified  $\sigma$  range when the fixed coordinates are compared with the coordinates redetermined using the corrupted TOA measurements. These plots clearly show that a corruption in the TOA measurements just as it is bound to happen in practice by means of interference, pulse distortion or unresolved multipath signals, has as expected a negative

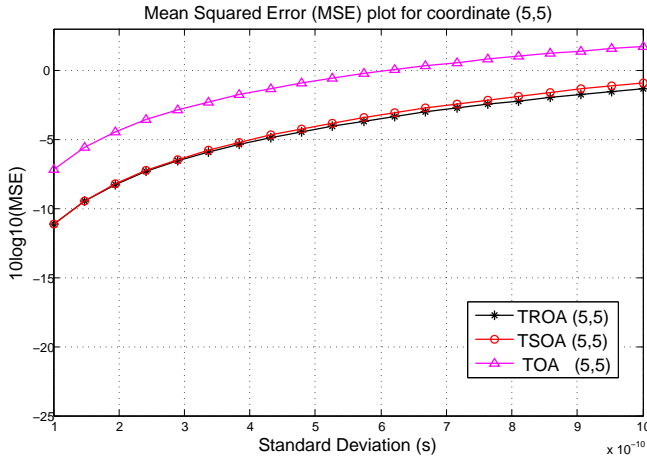


Fig. 10: Mean Squared Error (MSE) comparison for Coordinate (5,5)

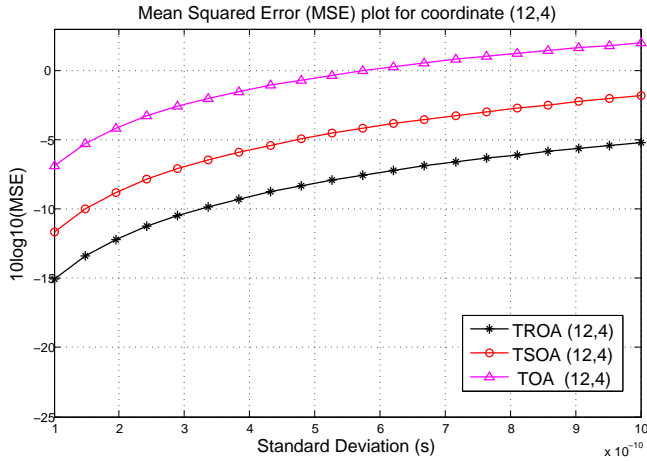


Fig. 11: Mean Squared Error (MSE) comparison for Coordinate (12,4)

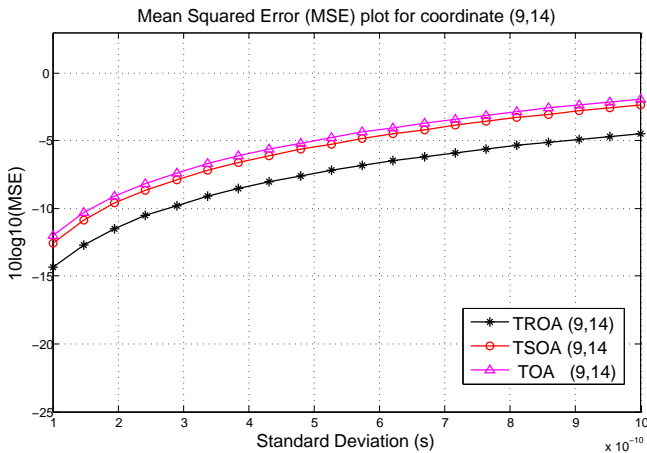


Fig. 12: Mean Squared Error (MSE) comparison for Coordinate (9,14)

effect on the localisation effectiveness on all three methods. In an apparent disagreement with literature, these plots also show that TSOA has a better performance than TOA. However,

this better performance is attributed to the extra receiver requirement TSOA needs to do the same positioning task as TOA (i.e., TSOA = 4  $R_x$  and TOA = 3  $R_x$ ); and hence backing up literatures statement that TSOA does not necessarily provide any additional performance advantages over existing multilateration techniques. Finally and most significantly, it is also clear to see that TROA will always have a better location estimation effectiveness in terms of MSE when compared to the other two methods over the defined  $\sigma$  range.

### B. Efficiency Test of TROA via CRLB

To study the efficiency of the proposed TROA approach, we compare the MSEs of the parameter estimation to their corresponding Cramér-Rao lower bounds (CRLBs). The CRLBs provide a lower bound on the covariance that is asymptotically achievable by any unbiased estimation algorithm based on the measurement vector  $\mathbf{z}$  [17]. It is calculated from the inverse of the Fisher Information Matrix (FIM)  $\mathbf{J}$ . Let the target location  $x \in \mathbb{R}^2$  be the parameter of interest and  $\hat{x}$  an estimate of it obtained from the measurement vector  $\mathbf{z}$ . Then the error covariance  $\mathbb{E}[(\hat{x} - x)(\hat{x} - x)^T]$  is bounded below by:

$$\mathbb{E}[(\hat{x} - x)(\hat{x} - x)^T] \geq \mathbf{J}^{-1} \quad (4)$$

$$\mathbf{J} = \mathbb{E}[\nabla_x \ln p(\mathbf{z}|x)(\nabla_x \ln p(\mathbf{z}|x))^T] \quad (5)$$

where  $\mathbb{E}[\cdot]$  determines the expectation value.

Additionally the unknown time of emission  $t_0$  is to be estimated. Therefore, for localisation, the parameter of interest is the extended position state of the emitter:

$$x^{(+)} = (t_0, x^T)^T \in \mathbb{R}^3 \quad (6)$$

Given the measurement vector  $\mathbf{z}_t$ , the CRLB for TROA localisation for one time step is computed from the inverse of the Fisher information for TROA, a  $3 \times 3$  matrix:

$$\mathbf{J}_t = \frac{\partial \mathbf{h}_t^T}{\partial x^{(+)}} \mathbf{R}_t^{-1} \frac{\partial \mathbf{h}_t}{\partial x^{(+)}} \quad (7)$$

The Jacobian of the measurement function is:

$$\frac{\partial \mathbf{h}_t}{\partial x^{(+)}} = \begin{pmatrix} \frac{\partial h_1}{\partial t_0} & \frac{\partial h_1}{\partial x} & \frac{\partial h_1}{\partial y} \\ \frac{\partial h_2}{\partial t_0} & \frac{\partial h_2}{\partial x} & \frac{\partial h_2}{\partial y} \\ \frac{\partial h_3}{\partial t_0} & \frac{\partial h_3}{\partial x} & \frac{\partial h_3}{\partial y} \end{pmatrix} = \begin{pmatrix} c & \frac{x-x_1}{r_1} & \frac{y-y_1}{r_1} \\ c & \frac{x-x_2}{r_2} & \frac{y-y_2}{r_2} \\ c & \frac{x-x_3}{r_3} & \frac{y-y_3}{r_3} \end{pmatrix} \quad (8)$$

The computation of the FIM follows as:

$$\begin{aligned} \mathbf{J}_t &= \begin{pmatrix} c & c & c \\ \frac{x-x_1}{r_1} & \frac{x-x_2}{r_2} & \frac{x-x_3}{r_3} \\ \frac{y-y_1}{r_1} & \frac{y-y_2}{r_2} & \frac{y-y_3}{r_3} \end{pmatrix} \times \begin{pmatrix} \frac{1}{\sigma_1^2} & 0 & 0 \\ 0 & \frac{1}{\sigma_2^2} & 0 \\ 0 & 0 & \frac{1}{\sigma_3^2} \end{pmatrix} \\ &\times \begin{pmatrix} c & \frac{x-x_1}{r_1} & \frac{y-y_1}{r_1} \\ c & \frac{x-x_2}{r_2} & \frac{y-y_2}{r_2} \\ c & \frac{x-x_3}{r_3} & \frac{y-y_3}{r_3} \end{pmatrix} \\ &= \sum_{i=1}^3 \begin{pmatrix} \frac{c^2}{\sigma_i^2} & \frac{c}{\sigma_i^2} \frac{x-x_i}{r_i} & \frac{c}{\sigma_i^2} \frac{y-y_i}{r_i} \\ \frac{c}{\sigma_i^2} \frac{x-x_i}{r_i} & \frac{1}{\sigma_i^2} \frac{(x-x_i)^2}{r_i^2} & \frac{1}{\sigma_i^2} \frac{(x-x_i)(y-y_i)}{r_i^2} \\ \frac{c}{\sigma_i^2} \frac{y-y_i}{r_i} & \frac{1}{\sigma_i^2} \frac{(x-x_i)(y-y_i)}{r_i^2} & \frac{1}{\sigma_i^2} \frac{(y-y_i)^2}{r_i^2} \end{pmatrix} \end{aligned} \quad (9)$$

The Fisher information can be expressed by:

$$\mathbf{J}_t = \begin{pmatrix} J_{11} & J_{12} & J_{13} \\ J_{21} & J_{22} & J_{23} \\ J_{31} & J_{32} & J_{33} \end{pmatrix} = \begin{pmatrix} J_t & J_{t,pos} \\ J_{pos,t} & \mathbf{J}_{pos} \end{pmatrix} \quad (10)$$

where  $\mathbf{J}_{pos}$  is the Fisher information of the position space,  $J_t$  The FIM of the time space and the others are the cross terms. The CRLB of the position space can be computed using the matrix inversion lemma [17]. The time of emission is treated as nuisance parameter. It can be shown that  $\mathbf{J}_{pos} = \mathbf{J}_{\Delta t_i}, i = 1, \dots, 3$ .

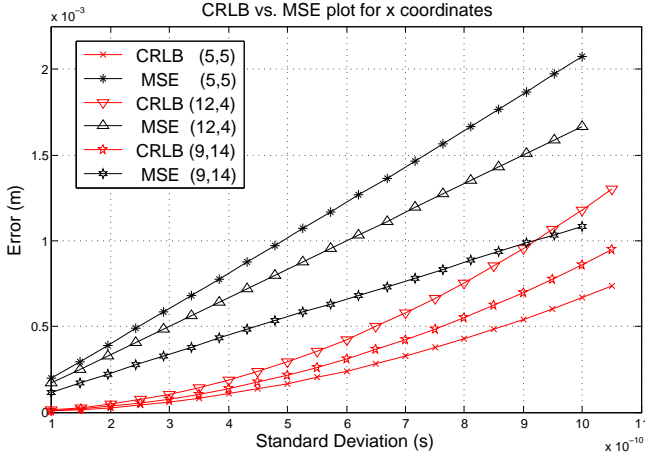


Fig. 13: CRLB vs. MSE comparison for x coordinates of (5,5), (12,4) and (9,14)

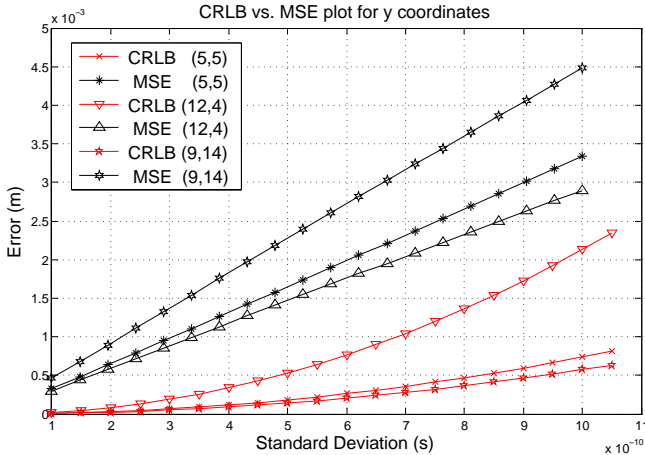


Fig. 14: CRLB vs. MSE comparison for y coordinates of (5,5), (12,4) and (9,14)

Fig. 13 and Fig. 14 illustrate the estimation performance of our approach for the  $x$  coordinate and  $y$  coordinate of the NOI, respectively. The localisation performance was studied for 3 different position of the NOI within the indoor environment of interest. We considered the following positions:  $(x, y) = (5, 5), (12, 4), (9, 14)$ . In these three cases, the TROA approach shows good performances where the MSEs are close to their respective CRLBs.

## VI. CONCLUSION

This paper presented a novel UWB driven multilateration technique for position estimation in an indoor environment. The presented approach exploits the inherent properties of UWB signal propagation; and its definition is in conjunction with the operational principles of the lesser studied TSOA position estimation technique. In this work we have studied the accuracy of the proposed approach for a network of three receivers and one transmitter. By means of a series of statistically driven MSE analyses, we have shown that in comparison with TOA and TSOA, the proposed TROA technique possesses a much higher accuracy with regards to position estimation. The CRLBs were also computed using TROA measurement set; and we have been able to show that the proposed TROA technique shows good performances when the CRLB is directly compared with the MSE. We have studied the influence of the position of the NOI within the indoor environment and relatively to the network of sensors. This latter study could be made more generic by varying the position of the NOI in a continuous fashion within the environment of interest which will provide a means of assessing optimum performances of our system.

## ACKNOWLEDGMENT

The authors would like to thank the Engineering and Physical Science Council (EPSRC) and DANCER project team at London South Bank University for their financial contribution towards this work.

## REFERENCES

- [1] I. Yamada, T. Ohtsuki, T. Hisanaga and Li Zheng, "An indoor position estimation method by maximum likelihood algorithm using RSS", *Annual Conference, SICE, 2007* pp.2927-2930, 17-20 Sept. 2007.
- [2] N. Uchitomi, A. Inada, M. Fujimoto, T. Wada, K. Mutsuura and H. Okada, "Accurate indoor position estimation by Swift-Communication Range Recognition (S-CRR) method in passive RFID systems", *International Conference on Indoor Positioning and Indoor Navigation (IPIN), 2010* pp.1-7, 15-17 Sept. 2010.
- [3] D. Hauschildt and N. Kirchhof, "Improving indoor position estimation by combining active TDOA ultrasound and passive thermal infrared localization", *8th Workshop on Positioning Navigation and Communication (WPNC), 2011* pp.94-99, 7-8 April 2011.
- [4] R. Hongliang, M.Q.-H Meng and X. Lisheng, "Indoor Patient Position Estimation Using Particle Filtering and Wireless Body Area Networks", *29th Annual International Conference of the IEEE Engineering in Medicine and Biology Society, EMBS 2007* pp.2277-2280, 22-26 Aug 2007.
- [5] M. Aso, M. Kawabata and T. Hattori, "A new location estimation method based on maximum likelihood function in cellular systems", *54th IEEE Conference on Vehicular Technology, VTC 2001* pp. 106- 110, vol.1, 2001.
- [6] K. Man-Kin Chu, J. Kee-Yin Ng and K. R.P.H.Leung, "A New Approach for Locating Mobile Stations under the Statistical Directional Propagation Model", *20th International Conference on Advanced Information Networking and Applications, AINA 2006* pp.932-940, 18-20 April 2006.
- [7] T. Roos, P. Myllymaki and H. Tirri, "A Statistical Modeling Approach to Location Estimation" *IEEE Trans. Mobile Comput.*, vol. 1, no. 1, pp. 59-69, Jan-Mar. 2002.
- [8] D. Munoz, F. Bouchereau, C. Vargas and R. Enriquez-Caldera, "Position Location Techniques and Applications", Academic Press, Elsevier Inc Publications, 2009.
- [9] Yunhao Liu and Zheng Yang, "Location, Localization, and Localizability: Location-awareness Technology for Wireless Networks", Springer Publications, 2011.
- [10] Luther Pfahler Eisenhart, "Coordinate Geometry (Reprint)", Dover Publications, 2005.



- [11] L. Kuen-Tsiar and C. Wei-Kai, "Mobile positioning based on TOA/TDOA/TDOA measurements with NLOS error reduction", *Proceedings of International Symposium on Intelligent Signal Processing and Communication Systems, ISPACS 2005*, pp. 545- 548, 13-16 Dec. 2005.
- [12] M. Ghavami, L. B. Michael and R. Kohno, "Ultra Wideband Signals and Systems in Communication Engineering", John Wiley and Sons Publications, 2004.
- [13] O. Onalaja and M. Ghavami, "UWB based pre-localisation algorithm for aiding target location in a multipath environment", *IEEE International Conference on Ultra-Wideband (ICUWB), 2011*, pp. 140-144, 14-16 Sept. 2011.
- [14] O. Onalaja, M. Ghavami and M. Adjrard, "UWB-based Elliptical Target Localization in an Indoor Environment", *8th International Workshop on Systems, Signal Processing and their Applications (WoSSPA)*, pp. 103-107, 12-15 May 2013.
- [15] R. C. Qiu, "A generalized time domain multipath channel and its application in ultra-wide-band (UWB) wireless optimal receiver design: system performance analysis", *IEEE Wireless Communications and Networking Conference (WCNC), 2004*, vol.2, no., pp.901- 907, 21-25 March 2004
- [16] R. C. Qiu, "A generalized time domain multipath channel and its application in ultra-wideband (UWB) wireless optimal receiver design-Part II: physics-based system analysis" *IEEE Transactions on Wireless Communications*, vol.3, no.6, pp.2312- 2324, Nov. 2004
- [17] S. M. Kay, "Fundamentals of Statistical Signal Processing: Estimation Theory", Prentice Hall Signal Processing Series, 1993.